AIAA–2000–0854
Generation of Bubbly Suspensions in Low Gravity

H.K. Nahra, M.I. Hoffmann, and S. Hussey
NASA Glenn Research Center
Cleveland, OH
and
K.R. Bell
Pennsylvania State University
University Park, PA

38th Aerospace Sciences Meeting & Exhibit
January 10–13, 2000 / Reno, NV

AIAA–2000–0854

GENERATION OF BUBBLY SUSPENSIONS IN LOW GRAVITY

Henry K. Nahra
NASA-Glenn Research Center
Lewis Field
21000 Brookpark Rd.
Cleveland, OH 44135
E-mail:
henry.k.nahra@grc.nasa.gov

Monica I. Hoffmann
NASA-Glenn Research Center
Lewis Field
21000 Brookpark Rd.
Cleveland, OH 44135
E-mail:
monica.i.hoffmann@grc.nasa.gov

Sam Hussey
NASA-Glenn Research Center
Lewis Field
21000 Brookpark Rd.
Cleveland, OH 44135
E-mail:
sam.hussey@grc.nasa.gov

Kimberly R. Bell
Chemical Engineering Department
Pennsylvania State University
University Park, PA
E-mail:
krb152@ psu.edu

Abstract

Generation of a uniform monodisperse bubbly suspension in low gravity is a rather difficult task because bubbles do not detach as easily as on Earth. Under microgravity, the buoyancy force is not present to detach the bubbles as they are formed from the nozzles. One way to detach the bubbles is to establish a detaching force that helps their detachment from the orifice. The drag force, established by flowing a liquid in a cross or co-flow configuration with respect to the nozzle direction, provides this additional force and helps detach the bubbles as they are being formed. This paper is concerned with studying the generation of a bubbly suspension in low gravity in support of a flight definition experiment titled "Behavior of Rapidly Sheared Bubbly Suspension." Generation of a bubbly suspension, composed of 2 and 3 mm diameter bubbles with a standard deviation <10% of the bubble diameter, was identified as one of the most important engineering/science issues associated with the flight definition experiment. This paper summarizes the low gravity experiments that were conducted to explore various ways of making the suspension. Two approaches were investigated. The first was to generate the suspension via a chemical reaction between the continuous and dispersed phases using effervescent material, whereas the second considered the direct injection of air into the continuous phase. The results showed that the reaction method did not produce the desired bubble size distribution compared to the direct injection of bubbles. However, direct injection of air into the continuous phase (aqueous salt solution) resulted in uniform bubble-diameter distribution with acceptable bubble-diameter standard deviation.

1. Introduction

Bubbly suspensions are crucial for mass and heat transport processes on Earth and in Space. These processes are relevant in pharmaceutical, chemical, nuclear and petroleum industries on Earth. They could also play an important role in NASA's future space missions life support, In-Situ Resource Utilization and propulsion processes for long duration space missions such as the Human Exploration and Development of Space (HEDS). Understanding the behavior of the suspension in Low gravity is crucial because of issues such as bubble segregation which could result in coalescence and could impact heat and mass transport. The physics of bubbly suspension is being studied by Sangani and Koch (1998). The aforementioned Principal Investigators plan to perform a microgravity experiment of shearing a bubbly suspension in a couette cell and comparing the bubble distribution in the couette gap to the one predicted by the suspension averaged equations of motion. The Behavior of Rapidly Sheared Bubbly Suspensions is a Fluids Physics Research experiment designed to validate a theory for predicting the effects of bubble interactions in inertial multiphase flows. To achieve this objective a uniform bubbly water suspension, must be produced in a couette cell in a microgravity environment. The volume fraction and velocity distribution in the suspension are measured as the outer cylinder is rotated at various speeds. Microgravity allows for pure shearing motion

without the effects of buoyancy. The forces acting on the bubbles in this configuration are the centrifugal force, which effectively pushes the bubbles toward the inner cylinder (due to the difference in densities between the dispersed and continuous phases), and the shear induced bubble pressure, which tends to push the bubbles apart from each other. This experiment will help further scientific understanding of multiphase flow and is applicable to boiling heat exchangers, bubble columns, distillation, secondary oil recovery, sediment transport and pipeline slurry transport.

In order to perform the experiment, a technology for generating a bubbly suspension in microgravity is to be established, tested and verified prior to the build-up phase of the flight experiment.

2. Early Bubbler Development

Two approaches for creating the bubbly suspension in low gravity conditions were explored. The first was to create bubbles from a chemical reaction of an effervescent material with water. The chemical reaction results in CO_2 bubbles formed in the continuous phase (water). The second was to directly inject air into water and detach the bubbles by inducing a relative motion between the bubble and the surrounding body of water, (Kim et. al., 1994). The two approaches are described in details below.

2.1 Bubbly Suspension Using Effervescent Material

Experiments to create a bubbly suspension using an effervescent material were conducted on board of the DC-9 aircraft low gravity platform. The bubbler consisted of a circular tablet of Alka-Seltzer™ fully coated/masked except in small areas of different shapes where the chemical reaction with water can take place. The tablet was spun in still water and the diameter of the generated CO_2 bubbles was measured. Such measurement of the bubble diameter showed variations that exceeded the 10% required by science requirements. Furthermore, the unknown kinetics of the chemical reaction and the solid residues that could result from such a reaction were of concern, as well as the sensitivity of the CO_2 solubility in water. This approach was thereby abandoned.

2.2 Bubbly Suspension by Direct Air Injection in Still Water

The approach of injecting air into the water using a nozzle resulted in different bubbler designs that were tested in low gravity. Cylindrical, T-shaped, sintered metal filter and capillary bubblers, depicted in Fig. 1 were tested. Air was injected into these bubblers from an air bottle. The bubblers were spun at different angular velocities and bubble generation was studied under different conditions involving air flow rate and spin speed. Figure 2 shows a gallery of the bubblers operating in still water. The most promising design was the capillary bubbler that consisted of a rotating body connected to a capillary through which air was injected into the liquid. The rotation was needed for establishing detachment in low gravity. This bubbler design was developed further for better control on the spin rate and gas flow rate. The spinning bubbler design, although showed promising results was rather difficult to implement in a couette cell system due to the rotating parts and their control. This realization led to the stationary bubbler design as implemented in the couette cell.

3. Development of the Couette System with Stationary Bubblers

The work described above was performed prior to the NASA Science Concept Review (SCR) of the flight definition project "Behavior of Rapidly Sheared Bubbly Suspension." After SCR and during the Requirement Definition Review (RDR) phase, a couette system was built and used as a test bed for testing bubbler concepts and the diagnostics for bubble collision frequency and void fraction measurements in the couette gap.

3.1 Hardware Description

The experiment rack included a couette assembly, which consisted of a couette, a drive motor, a bubbler, and a hot wire probe anemometer. Magnesium sulfate ($MgSO_4$) salt was added to the water in the couette to create a 0.05 molar solution to inhibit bubble coalescence. The couette was designed to hold approximately 3 liters of water between the inner and outer cylinders. The couette gap width was 3 cm and the height 10 cm. The outer cylinder is optically clear (acrylic), and capable of spinning from 0-100 rpm driven by a 1/2 HP motor with a DC speed controller. The couette inner cylinder, also acrylic, was stationary.

The acrylic top and stainless steel bottom of the couette rotated with the outer cylinder. The couette seal material was made of a polymer filled Teflon™. A tachometer, pressure transducer, and a type K thermocouple were added to the couette assembly.

3.1.1 Bubble Injection

Bubbles were produced in the couette through a capillary tube attached to the couette inner cylinder. Figure 3 shows a flow diagram of the bubble injection process. Three different capillary sizes were tested, one size per day (0.031, 0.041, and 0.051 cm diameters).

A piston-type 2.54 cm ID pump equipped with a ¼ HP was used to remove water from the couette while pumping air in through the bubbler. An air flow meter (0-50 sccm) was added to the air line. Operating in the reverse direction, the same pump was used to remove air from the couette while replacing the water.

3.1.2 Separation and Fluid Re-circulation

A re-circulation system (Fig. 3) was used during the high-g period to remove any remaining air from the top of the couette. This was accomplished by pumping water into the bottom of the couette from an accumulation tank using a 12VDC marine pump. The pump was actuated from a momentary toggle switch. The acrylic accumulation tank was designed to hold approximately 750 milliliters of fluid and was vented to atmosphere through a long 0.317 cm diameter tube, connected to a ½ liter squeeze bottle. The system was designed to run at ambient pressure. A 27.6 KPa relief was attached to the test chamber to protect the system in the event of a rapid cabin depressurization. The flow system contained approximately 3 liters of 0.05-molar salt ($MgSO_4$) water solution.

3.1.3 Diagnostics Testing

A hot wire probe anemometer was used to test the dynamics of bubble-probe collision. The probe was mounted just downstream of the bubbler, attached to the inner cylinder with the probe head positioned in the flow field. The hot wire probe was monitored and controlled via a notebook computer attached to an expansion chassis.

3.1.4 Visualization

An S-VHS high speed (1000 frames/s) camera and four standard 30 frames/second video cameras were used to view the experiment. Three of the standard speed video cameras were identical, industrial black and white cameras. Two of the video cameras were mounted above the couette to get a top view of the bubbles near the bubbler and the hot wire probe respectively. The third video camera was focused on the outside of the couette to view both the bubbler and the hot wire probe together. The fourth standard speed video camera was a handheld color camcorder, mounted to the rig support structure via a quick-disconnect-type mount to get an overall view of the couette. The high speed camera was mounted above the couette and focussed on a mirror to view the bubbles coming from the bubbler. The couette lighting consisted of a 120VAC fiber optic light source, which illuminated the couette bottom by reflecting light through a frosted angled ring mounted inside the couette.

3.1.5 Time Synchronization

All four industrial cameras, the hot wire probe anemometer, the pressure, temperature, tachometer, and airflow readings were time synchronized via a time-code generator mounted on the video rack. The high speed video camera was not time synchronized with the rest of the data acquisition.

3.2 Test Matrix

The test matrix followed in this series of experiments on board of the KC-135 is shown in table 1. Experiments of suspension generation were carried out under 4 rotational speeds and three different gas flow rates and for three orifice diameters located at 0.25, 0.5 and 0.75 cm from the inner wall. The objective was to explore a wide range of parameters and search for the optimum ones that result in acceptable bubble diameter and standard deviation.

4. Results and Discussion

4.1 Spinning Bubblers in Still Fluid

Figure 4 shows a summary of the bubble diameter as a function of local liquid relative velocity and the air flow rates. The trend of the data shows that as we increase the spin velocity of the bubbler, the bubble diameter decreases due to the higher drag force acting on it. Furthermore, as we increase the gas flow rate, the bubble diameter increases at a specific local liquid velocity, unlike what was observed in the bubble injection experiments in still water and under low gravity conditions, performed by Pamperin et. al. (1994). Pamperin showed that as the gas flow rate increases, the bubble diameter decreases as bubbles form under low gravity in still volume of water. The regime of bubble formation and detachment in Pamperin's study was

controlled by the high momentum flux force. This force encouraged early bubble detachment. Moreover, in the Pamperin study, there was no liquid velocity imposed on the forming bubble and the only drag force was due to bubble expansion into the fluid. From the trend of the bubble diameter versus the gas flow rate, there seems to be a combination of forces that cause a delay in the detachment time and thereby results in larger bubbles. Bubbles formed from this bubbler showed a standard deviation less than 10% of the average diameter. Although this bubbler design showed promising results, the effects of spinning the bubbler in to the fluid will result in a rather complicated flow field which will render the determination of the local velocity at the bubbler tip difficult if not impossible. Consideration of both, the engineering implementation of the spinning bubbler and the induced flow field issues led us to investigate and implement the stationary bubbler design.

4.2 Stationary Bubbler in a Couette Cell

Results of bubble formation and suspension generation experiments using the couette cell described above are shown in figures 8 through 11 where the bubble diameter is plotted as a function of the calculated fluid velocity in the couette at a particular radial position. Before we analyze the figures, we will discuss the approach to answer several questions regarding the experiment variables.

4.2.1 Estimation of Liquid Velocity

The local liquid velocity was calculated from the velocity profile equation in a couette cell given by (Schlichting, 1955):

$$u(r)=\frac{1}{r_2^{\,2}-r_1^{\,2}}\left[\alpha r-\frac{\beta}{r}\right] \qquad (1)$$

where r_1 and r_2 are the radii of the inner and outer couette shells, and α and β are two constants given in terms of the rotation speeds, ω_1 and ω_2 and the radii of the inner and outer shells, namely:

$$\alpha=\omega_2 r_2^{\,2}-\omega_1 r_1^{\,2} \qquad (2)$$

$$\beta=r_1^{\,2} r_2^{\,2}(\omega_2-\omega_1) \qquad (3)$$

In our experiment, ω_1 was zero because the inner shell of the couette was stationary. This steady state equation governing the velocity distribution in a couette cell was used to approximate the velocity of the fluid at a specific radial position r. Direct measurement of the liquid velocity is planned for future experiments using the hot wire anemometer. The latter will also be utilized to measure the bubble collision frequency in the couette gap as well. It is assumed in equation 1 that the end effects of the couette are negligible. The span of the liquid velocity range is based on different bubbler-tip radial locations in the couette and different rotational speeds. The radial locations were 0.25 cm, 0.5 cm and 0.75 cm from the stationary inner wall of the couette cell. The angular speed of the couette outer shell ranged from 10 to 40 rpm.

4.2.2 Initial Waiting Time to Approach Steady State

The time to approach steady state was calculated using the unsteady state solution of the Stoke's first problem applied to a fluid between two boundaries with one stationary and the other is set to a velocity U_1 at $t > 0$. For simplicity, rectangular coordinates were used in this calculation. The solution to this problem is given in terms of a Fourier series (Powers, 1972), namely,

$$u(y,t)=U_1\frac{y}{h}+\frac{2}{\pi}U_1\sum_{n=1}^{\infty}\frac{(-1)^n}{n}Sin\left[\frac{n\pi y}{h}\right]e^{-\left(\frac{n\pi}{h}\right)^2 \nu t} \qquad (4)$$

where h is the separation between the two plates and the distance y from the stationary plate, and ν is the kinematic viscosity of the liquid phase and t is the time. Based on equations 4 an initial waiting time of 5 minutes would establish a liquid velocity distribution that is less that 7% of the steady velocity distribution. Figure 5 shows the developing velocity profile in a couette flow. The velocity U_1 was taken as 10 cm/s and the couette gap h as 3 cm.

4.2.3 Waiting Time between Low Gravity Periods

To assess the effects of the waiting time between low gravity periods on the developing velocity profile, the Stoke's first problem was solved. The initial condition of the problems was that the flow is fully developed at $t<0$. The boundary conditions were that the velocity is zero at one plate and U_2 at the moving plate. The solution is given by:

$$u(y,t)=U_2\frac{y}{h}+\frac{2}{\pi}(U_2-U_1)\sum_{n=1}^{\infty}\frac{(-1)^n}{n}Sin\left[\frac{n\pi y}{h}\right]e^{-\left(\frac{n\pi}{h}\right)^2 \nu t} \qquad (5)$$

Figure 6 shows the transient developing flow when the moving plate is suddenly accelerated from U_1 to U_2, where U_1 is taken as 10 cm/s and U_2 as 20 cm/s. These velocities are typical of the experiment performed on the KC-135 low gravity platform aircraft.

4.2.4 Data Analysis and Uncertainties

Figure 7 shows a top view of the couette cell as bubbles were being produced from the bubbler that is inserted into the flow. The air flow rate Qg is on the order of ~20 cc/min, inner orifice diameter D_N of 0.051 cm and the liquid velocity $U=u(0.25cm)$ as estimated by equation 1 on the order of 3 cm/s.

Figure 8 shows the bubble diameter as a function of the liquid velocity in the couette as estimated by equation 1, for a nozzle diameter of 0.031 cm. The wide range of liquid velocity is accomplished by considering the range of rotational speeds of the outer shell at the various radial locations of the bubblers which were 0.25, 0.5 and 0.75 cm from the stationary wall. We note that as the couette rotational speed is increased, the bubble diameter is decreased because of the increased drag force applied on the bubble as it develops from the orifice. This increased drag force prevents the bubble from further developing and results in earlier detachment. Also, earlier detachment can be attributed to the increased lift force that increases with the shear rate that in turn increases when the rotational speed increases. The high speed video images were analyzed using the *TRACKER* software developed at NASA Glenn Research Center at Lewis Field by Klimek et. al. 1996, which allows to make bubble diameter measurements as well as tracking developing interfaces. Bubble diameter measurements were made over the middle of the low gravity period. The reason is to avoid any possibility of adverse acceleration levels experienced early and late during the low gravity maneuver. Some of the scenes however, were analyzed over the entire low gravity period. The gas flow rates in the figure 8 ranged from 3.5 to over 20 cc/min.

Figures 9 through 11 show that bubble diameter plotted as a function of the calculated liquid velocity for bubbles generated from the three nozzle diameters of 0.031, 0.041 and 0.051 cm. We see from the figures that in order to produce bubbles in the range between 2 and 3 mm, we need to operate at lower liquid velocities (2 to 8 cm/s) and gas flow rates (9 to 16 cm^3/min). The higher uncertainties (error bars) on the bubble diameter in figure 10 are probably caused by the fluctuation of the gas flow rate, and bubble sampling for bubble diameter measurements over the entire low gravity period.

Although the air flow rate was well characterized on ground, the acquired air flow data from flight show fluctuation in the flow rates during the 20 seconds of low gravity. This could be due to the dynamics of bubble formation and the effects of the "Chamber Volume" that influences the compressibility of gas as it is being discharged from the nozzle. It can also be due to some variation in the cabin pressure as the KC-135 travels the apex of the parabola, or to the presence of the check valve in the air line. The ground characterization of the air flow meter consisted of measuring the air flow for different settings of the motor speed that drives the piston pump. An acquired sample of the air flow rate data is shown in Fig. 12. The conditions for this scene are U_L=4.23 cm/s, D_N=.041 cm and the bubble produced have an average diameter D_B of 2.45 mm. The prescribed flow rate is 12 cc/min, however, figure 12 shows that the acquired flow rate is lower than 12 cc/min and fluctuates around 9 cc/min. The flow rates reported in the paper were the ones acquired by the data acquisition system and averaged over the low gravity period.

The calculated liquid velocity that was used in the plots of Fig. 9 through 11 uses equation 1 that assumes steady state conditions and no end effects. The assumption is not valid when the waiting period between runs is less than 5 minutes. As shown in Fig. 6, for a waiting period of 1 minute between parabolas/runs, the difference between the profiles of the steady and transient solution can be significant. In the present configuration, the couette end effects can not be neglected, which necessitates a 3D CFD analysis in order to fully understand the flow field of the continuous phase in the couette. Some insight can be gained into this issue if one looks at the unsteady state solution of the problem of suddenly accelerating two parallel plates to reach the same velocity U. The solution to this problem is given by,

$$u(y,t)=U-\frac{U}{\pi}\sum_{n=1}^{\infty}\frac{1-(-1)^n}{n}Sin\left(\frac{n\pi y}{h}\right)e^{-\left(\frac{n\pi}{h}\right)^2 vt} \qquad (6)$$

Figure 13 shows the unsteady state profiles for different times with the separation taken as 10 cm, which is the same as the couette height. One sees that at t=100 s which is nearly equivalent to the time between parabolas, the influence of the boundary layer depth does not reach the middle of the separation and thereby does not influence the local velocity. However, at 100 s, the velocity profile induced by the spinning outer shell which is at 3 cm from the stationary wall is significantly different from the steady state profile at

t=1000 s. Therefore, an optimum time for waiting between runs needs to be determined in order to minimize the difference between the transient velocity profiles along the couette gap, while keeping the contribution of the moving top and bottom moving plates to a minimum. To resolve the velocity issue, the hot wire anemometer intended for use to measure the bubble local concentration in the couette gap (by measuring collision frequency with probe), will be used in the future to calibrate the velocity profile in the couette cell gap.

The data shown in Fig. 9 through 11 exhibit a trend that is seen by several investigators (Bhunia et. al.1998, Nahra et. al. 1998). The nozzle diameter as shown in these figures plays an important role in determining the bubble diameter at detachment. The uncertainties in some of the data points can be attributed to the fluctuation in the gas flow, which can be in turn attributed to the bubble formation process, and to the sampling procedure in the data reduction process. It is worth noting, however, that the bubble diameter obtained from this experiment and the calculated standard deviations show that for most of the runs the bubble size is uniform, within the 10% standard deviation requirement set by the Science Requirement Document of the experiment.

5. Concluding Remarks

We presented in this paper the results of the effort aimed toward the generation and establishment of a bubbly suspension in low gravity. This effort is in support of the flight experiment titled "Behavior of Rapidly Sheared Bubbly Suspension." These results included the characterization of bubbles generated by various bubbler designs, which encompassed the spinning and stationary bubblers. Data scattering was thought to be due to the air flow rate fluctuations, the uncharacterized velocity profile inside the couette cell gap, and the method of data reductions for some of the runs. We also concluded that the air flow rates and liquid velocities should be small in order to produce bubbles within 2 and 3 mm in diameter. This is shown in Fig. 9 through 11. Future work encompasses continuing the data analyses of later experiments of suspension generation performed on board of the KC-135 Low Gravity Aircraft. These data analyses include the determination of the bubble diameter under different conditions of couette spin and gas flow rate, the experimental determination of the gas flow rate from bubble volume and time to detachment measurements, and the operation of the suspension diagnostics. These include the hot wire anemometer and impedance probes, which are intended to measure the bubble concentration and bubble speed respectively. Moreover, future plans include investigation of methods to remove the suspensions from the couette cell.

Acknowledgement

The authors wish to acknowledge the engineering team that worked diligently to build the test rig, and the KC-135 flight staff that made possible to perform the experiments. The authors wish to recognize the contributions of the student interns, Mr. Ryan Steiner, Mr. Diego Rhodes and Mr. Bassem Haddad who supported the data reduction and analyses.

References

Bhunia, A., Pais, S., Kamotani, Y., and Kim, I., Bubble "Formation in a Co-Flow Configuration in Normal and Reduced Gravity," *AIChE Journal*, 44, 1499–1507, 1998.

Kim, I., Kamotani, Y., and Ostrach, S. (1994) "Modeling of Bubble and Drop Formation in Flowing Liquids in Microgravity," *AIChE Journal* 40, 19–28.

Klimek, R.B., Wright, T.W., and Sielken, R.S. (1996) "Color Image Processing and Object Tracking System" NASA TM–107144.

Koch, D., and Sangani, A., "Science Requirement Document for Behavior of rapidly Sheared Bubbly Suspensions", August 1998.

Nahra, H., Kamotani, Y., "Bubble Formation and Detachment in Liquid Flow Under Normal and Reduced Gravity," AIAA–98–0732, 1998.

Pamperin, O., and Rath, H. (1995) "Influence of Buoyancy on Bubble Formation at Submerged Orifices" *Chem. Engn. Sci.* 50, 3009–3024.

Powers, D.L., "Boundary Value Problems", Academic Press, New York, 2nd edition, 1979.

Schlichting., H., "Boundary-Layer Theory", McGraw-Hill Inc., New York, 7th edition, 1987.

Couette angular velocity range
$0<\Omega_C<50$ rpm,
Ω_C =10, 20, 30, 40 rpm

Air Flow range, Q_B
3 settings, Q_{B1}, Q_{B2}, Q_{B3} where $1<Q_B<50$ cc/min

Bubbler Nozzle inner diameter
D_{N1} = 0.31 mm
D_{N2} = 0.41 mm
D_{N3} = 0.51 mm

			Ω_C		
		10	20	30	40
	Q_{B1}	1	6	7	12
Q_B	Q_{B2}	2	5	8	11
	Q_{B3}	3	4	9	10

Table 1. Test Matrix for the bubbly suspension generation experiments.

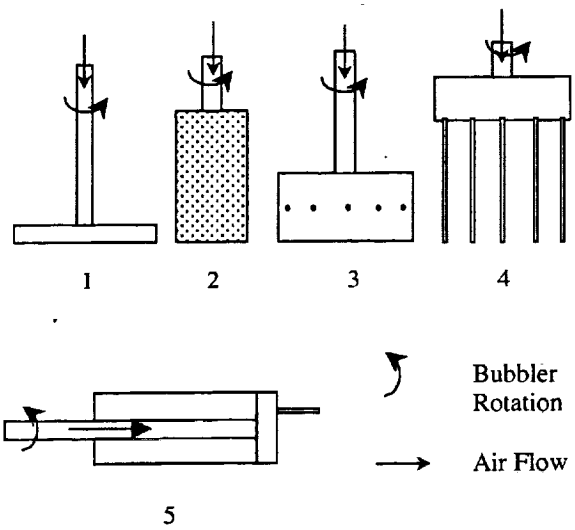

Figure 1. Various bubble design used in early experiments of suspension generation. 1. T-shape, 2. Sintered metal, 3. Cylindrical, 4. Capillary, and 5. Improved capillary bubblers.

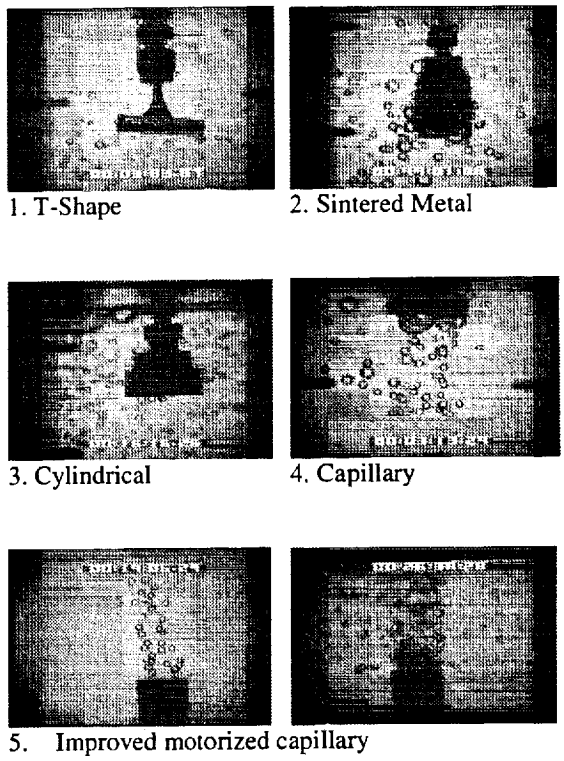

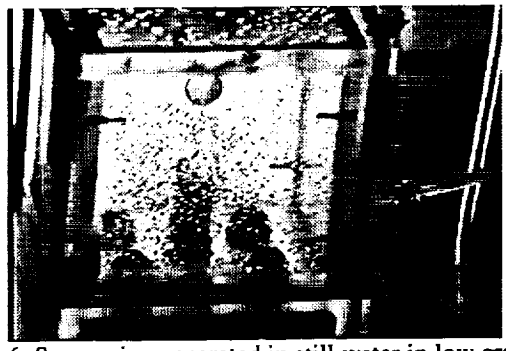

Figure 2. Gallery of bubblers tested during the early experiments of suspension generation.

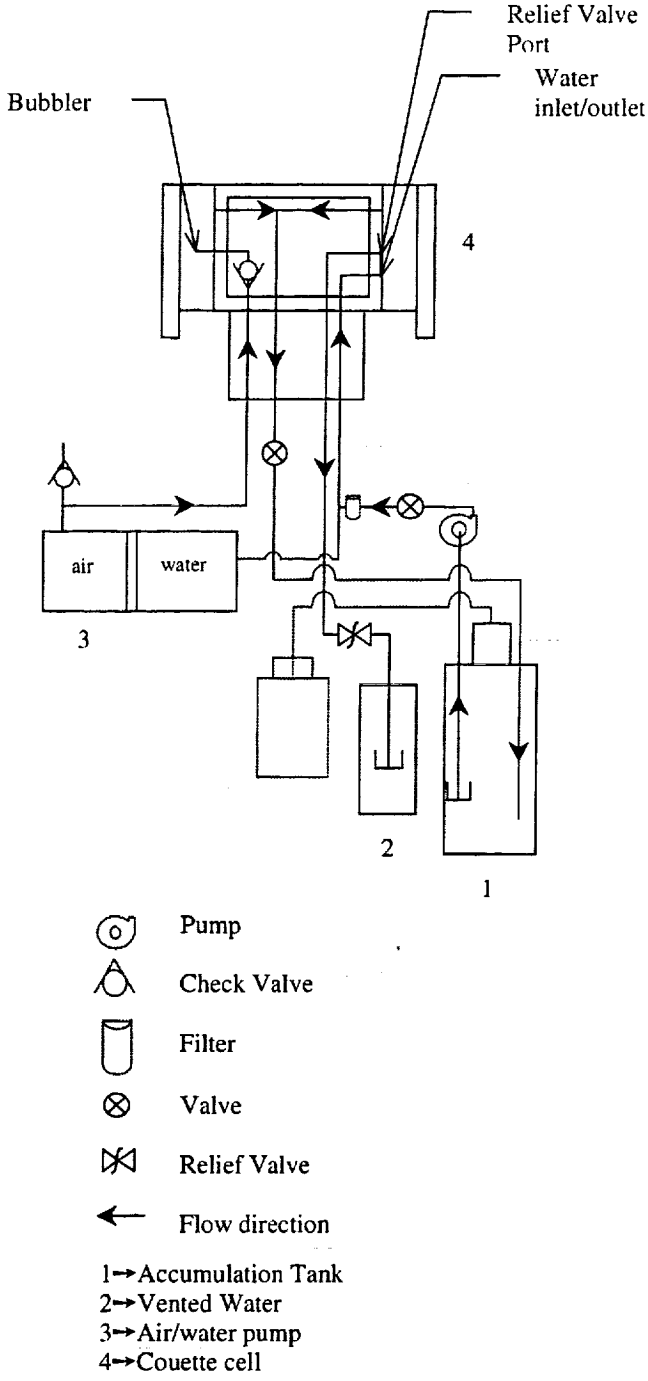

Figure 3. Simplified flow diagram of the bubbly suspension generation experiment.

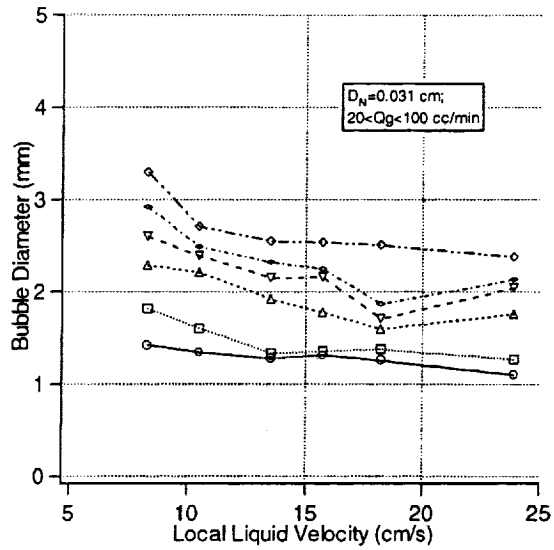

Figure 4. Summary of the bubble diameter as a function of local liquid relative velocity and the air flow rates for the spinning bubbler design.

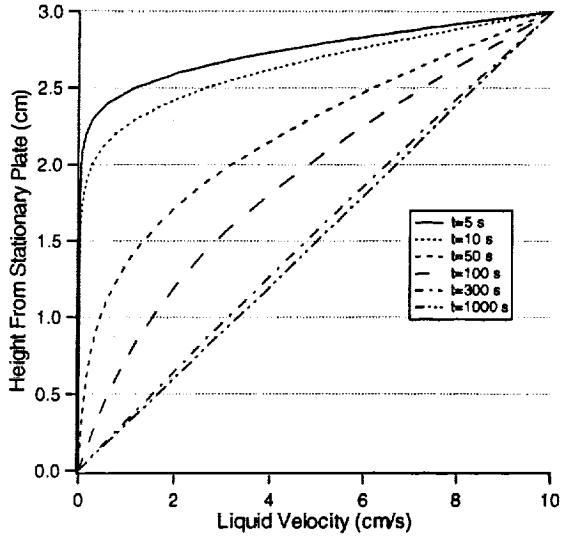

Figure 5. Transient velocity profile in a couette flow when the upper plate is suddenly accelerated from 0 to U_J=10 cm/s.

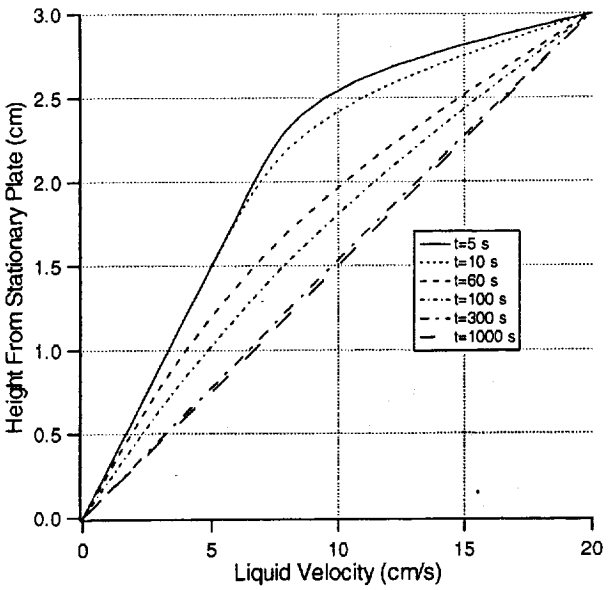

Figure 6. Transient velocity profile in a couette flow when the upper plate is suddenly accelerated from U_1=10 cm/s to U_2=20 cm/s.

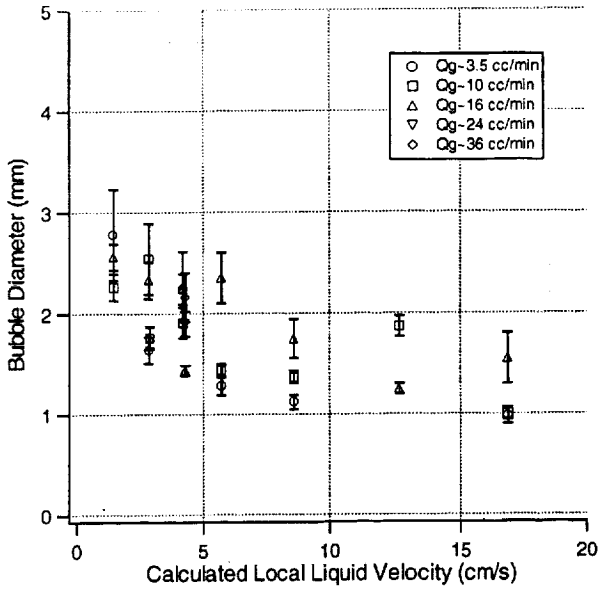

Figure 8. Bubble diameter as a function of calculated liquid velocity for D_N=0.031 cm.

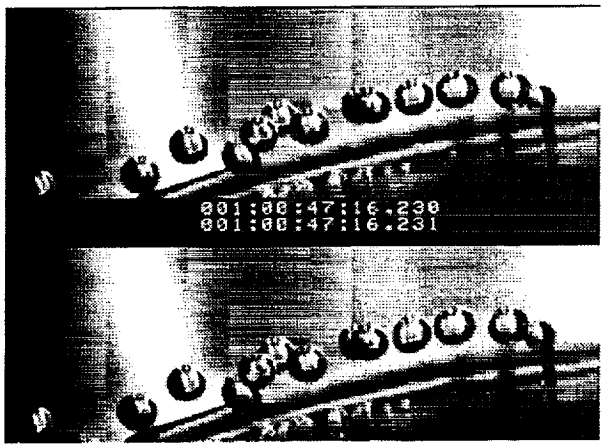

Figure 7. Bubble formation and detachment from a nozzle in a cross shear flow. Qg=20 cc/min, D_N=.051 cm and U_L=3 cm/s.

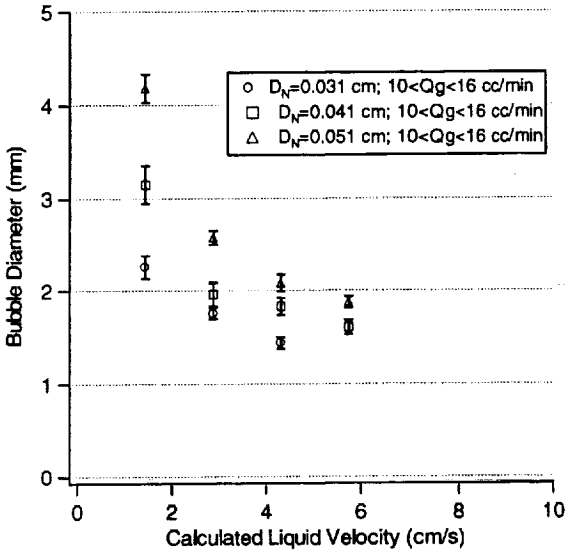

Figure 9. Bubble diameter as a function of the calculated liquid velocity for a bubbler tip location of d=0.25 cm, and 10<Qg<16 cc/min.

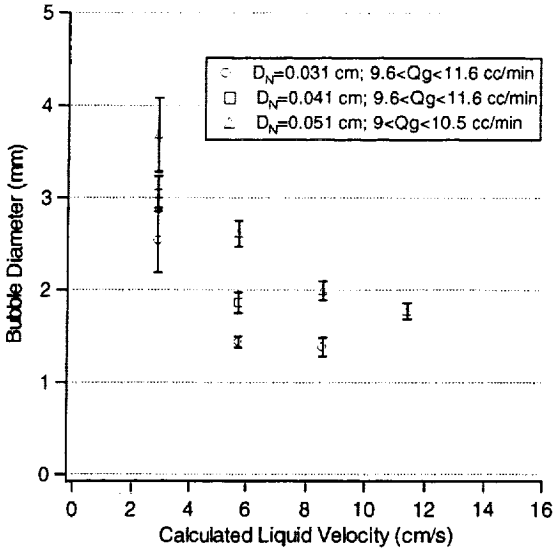

Figure 10. Bubble diameter as a function of the calculated liquid velocity for a bubbler tip location of d=0.5 cm, and 9<Qg<12 cc/min.

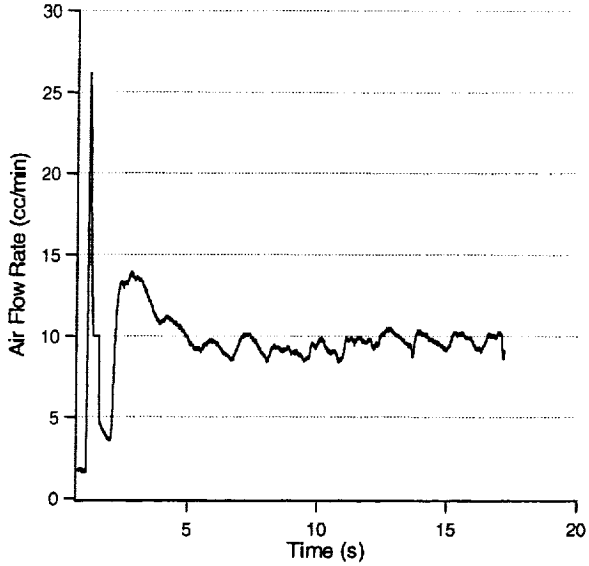

Figure 12. Acquired flow rate from the data acquisition showing the flow rate as a function of time during the low gravity period.

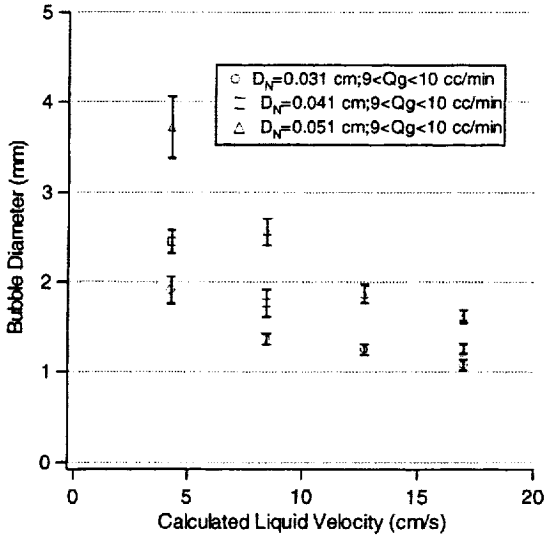

Figure 11. Bubble diameter as a function of the calculated liquid velocity for a bubbler tip location of d=0.75 cm, 9<Qg<10 cc/min.

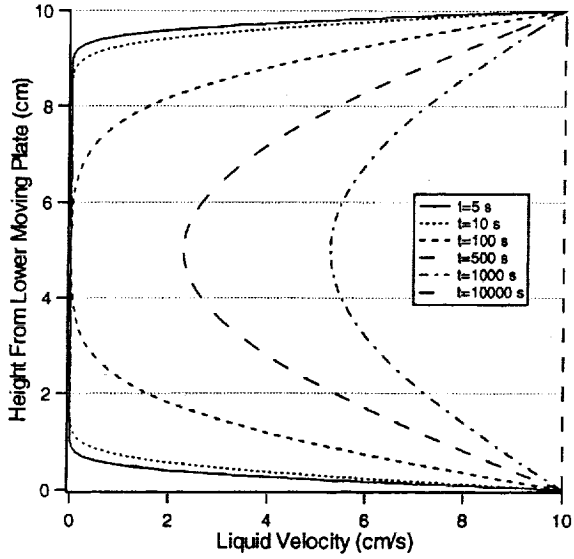

Figure 13. Transient velocity profile for the problem of two suddenly accelerated plates with a fluid in between. The separation l=10 cm and the velocity U=10 cm/s.